



**HAL**  
open science

# Ammonium aluminium carbonate hydroxide $\text{NH}_4\text{Al}(\text{OH})_2\text{CO}_3$ as an alternative route for alumina preparation: Comparison with the classical boehmite precursor

Robin Lafficher, Mathieu Digne, Fabien Salvatori, Malika Boualleg, Didier Colson, François Puel

## ► To cite this version:

Robin Lafficher, Mathieu Digne, Fabien Salvatori, Malika Boualleg, Didier Colson, et al.. Ammonium aluminium carbonate hydroxide  $\text{NH}_4\text{Al}(\text{OH})_2\text{CO}_3$  as an alternative route for alumina preparation: Comparison with the classical boehmite precursor. Powder Technology, 2017, 320, pp.565 - 573. 10.1016/j.powtec.2017.07.080 . hal-01654472

**HAL Id: hal-01654472**

**<https://centralesupelec.hal.science/hal-01654472>**

Submitted on 4 Dec 2017

**HAL** is a multi-disciplinary open access archive for the deposit and dissemination of scientific research documents, whether they are published or not. The documents may come from teaching and research institutions in France or abroad, or from public or private research centers.

L'archive ouverte pluridisciplinaire **HAL**, est destinée au dépôt et à la diffusion de documents scientifiques de niveau recherche, publiés ou non, émanant des établissements d'enseignement et de recherche français ou étrangers, des laboratoires publics ou privés.

This Accepted author version available online: 29 July 2017.

**To cite this article:** Robin Lafficher, Mathieu Digne, Fabien Salvatori, Malika Boualleg, Didier Colson, Francois Puel (2017) Ammonium aluminium carbonate hydroxide  $\text{NH}_4\text{Al}(\text{OH})_2\text{CO}_3$  as an alternative route for alumina preparation: comparison with the classical boehmite precursor. Powder Technology, 320, 565-573, DOI: 10.1016/j.powtec.2017.07.0080

## Ammonium aluminium carbonate hydroxide $\text{NH}_4\text{Al}(\text{OH})_2\text{CO}_3$ as an alternative route for alumina preparation: comparison with the classical boehmite precursor

Robin Lafficher<sup>a,b</sup>, Mathieu Digne<sup>a,\*</sup>, Fabien Salvatori<sup>a</sup>, Malika Boualleg<sup>a</sup>, Didier Colson<sup>b</sup> and François Puel<sup>c</sup>

<sup>a</sup> IFP Energies Nouvelles ; BP 3, F-69360 Solaize, France

<sup>b</sup> Univ Lyon, Université Lyon 1, CNRS, UMR5007, LAGEP, F-69622 LYON, France

<sup>c</sup> LGPM, CentraleSupélec, Université Paris-Saclay, F-92295 Châtenay-Malabry, France

\*Corresponding author Tel: +33 4 37 70 26 22

Email: [mathieu.digne@ifpen.fr](mailto:mathieu.digne@ifpen.fr) (Mathieu Digne)

### Abstract

Ammonium aluminium carbonate hydroxide (AACH) is a promising alternative precursor for preparation of alumina with high purity and original textural properties. In this paper, both boehmite (classical alumina precursor) and AACH were precipitated in a stirred tank reactor with close process parameters. Preparation protocols were thus compared. Main differences between both protocols were pointed out (reactant molar ratio influence, alumina concentration, filtration / washing step). This study helps for the choice of the appropriate preparation route for alumina precursor synthesis. As-synthesized boehmite and AACH precursors were then calcined between 500 °C and 1000 °C. The textural properties of the corresponding aluminas were characterized. At 500 °C, AACH-derived alumina revealed to be particularly porous, with larger mean pore diameter (*ca.* 29 nm) than boehmite-derived alumina (*ca.* 6 nm). Moreover, AACH-derived alumina exhibited a high surface area. However, a more accurate analysis revealed that this high specific surface area (407 m<sup>2</sup>.g<sup>-1</sup>) is mostly due to microporosity formation during the calcination step. At higher calcination temperature, boehmite and AACH-derived aluminas exhibited different behaviors against sintering. In particular, the latter showed an interesting ability to maintain a constant mean pore diameter, regardless of the calcination temperature.

**Keywords:** Precipitation, alumina, AACH, boehmite, sintering

### 1. Introduction

Supported heterogeneous catalysts are widely used in refining and petrochemical processes. One way to get better catalyst performances is to develop supports with enhanced properties. Due to its high surface area, as well as good mechanical, chemical and thermal stability,  $\gamma\text{-Al}_2\text{O}_3$  is often used as a catalyst support [1,2]. It is obtained by precursor dehydration, generally boehmite  $\gamma\text{-AlOOH}$ . However, even if further steps (shaping, thermal treatment) are used to adjust the final properties of alumina supports, the textural properties are to a large extent fixed by those of the initial solid precursor. A precise control of the support properties is also important to fit with a given refining process.

Various synthesis routes are possible for boehmite, such as sol-gel or aqueous precipitation processes, each leading to different ranges of textural properties and purity levels [2,3]. Very pure boehmite can be prepared by the sol-gel process using aluminium alkoxides [4], leading to alumina exhibiting low sodium content (< 40 ppm  $\text{Na}_2\text{O}$ ) [1,2] and surface area in the range of 200-500 m<sup>2</sup>.g<sup>-1</sup> [5]. However, precipitation of aluminium salts is a cheaper way to produce boehmite at an industrial scale. Several aluminium salts can be used ( $\text{Al}(\text{NO}_3)_3$ ,  $\text{AlCl}_3$ ,

$\text{Al}_2(\text{SO}_4)_3 \text{NaAlO}_2$ ) and their nature and concentration can have great influence on the morphology and textural properties of the precipitated particles [6]. Aluminas manufactured by precipitation generally exhibit surface area lower than  $300 \text{ m}^2 \cdot \text{g}^{-1}$  [3,7] and may have high impurities content (200-3000 ppm  $\text{Na}_2\text{O}$ ) [1,2].

Ammonium aluminium carbonate hydroxide (AACH, with formula  $\text{NH}_4\text{Al}(\text{OH})_2\text{CO}_3$ ), also called  $\text{NH}_4$ -dawsonite, can be an interesting alternative choice for preparation of  $\gamma\text{-Al}_2\text{O}_3$  with high purity level and new textural properties. Various methods can be used to synthesize AACH [8], but the main one remains the precipitation of aluminium salts ( $\text{Al}(\text{NO}_3)_3$ ,  $(\text{NH}_4)\text{Al}(\text{SO}_4)_2$ , or  $\text{AlCl}_3$ ) in aqueous phase with precipitating agents such as  $(\text{NH}_4)_2\text{CO}_3$  or  $\text{NH}_4\text{HCO}_3$  [9,10]. Influence of several parameters on the product properties have been studied so far: reactants [11], contacting mode [12–15], pH [16,17], molar ratio [9,15,18], alternative medias [17,19]. A wide range of  $\gamma$ -alumina textural properties have thus been described in the literature, with surface area ranging from 200 to  $500 \text{ m}^2 \cdot \text{g}^{-1}$ , as well as pore volume ranging from 0.7 to more than  $2.0 \text{ cm}^3 \cdot \text{g}^{-1}$ .

We observed in the literature that AACH is generally compared to boehmite from a textural point of view exclusively. However, since these two precursors can exhibit a different behaviour due to their particular properties [20], their preparation steps cannot be considered as being equivalent. Synthesis of pure AACH or boehmite thus requires certain specificities that need to be taken into account to compare the interest of both precursors from a more global perspective.

In the present work, a simple precipitation process in a double-jet stirred tank reactor was studied at the 2-4 liter scale. The preparation method was based on an optimized protocol for boehmite synthesis, and was adapted to AACH synthesis. By optimized protocol, we mean a protocol leading after calcination to  $\gamma$ -alumina material with high surface area (typically  $250\text{-}300 \text{ m}^2/\text{g}$ ) and high pore volume (typically  $0.8\text{-}0.9 \text{ cc/g}$ ), properties that are suitable for catalyst support. Precipitation of both precursors in similar conditions allowed us to point out the main specificities in each protocol. Then, boehmite, AACH and their derived aluminas were characterized in order to compare the thermal evolution of their textural properties. Finally we propose a proper comparison between two precursors to prepare porous alumina: the classical precursor one, boehmite, and a most original one, AACH. This consistent comparison between boehmite and AACH is performed both in terms of product properties and preparation advantages / disadvantages. In addition, the present work also proposes an interpretation to explain the strong increase in specific surface area generally observed during AACH calcinations.

## 2. Experimental

### 2.1 Synthesis of boehmite

The experimental setup is displayed on Figure 1. The boehmite synthesis is derived from the protocol reported by Morgado et al. [21]. Reagent grade aluminium sulphate (Univar) and sodium aluminate (Sigma-Aldrich) were used as starting materials without further purification.

The synthesis was carried out in a stirred tank reactor equipped with a mechanical stirrer and containing a 1170 mL initial water volume. Boehmite was precipitated by simultaneous dosing of an aluminium sulphate solution (acid reactant,  $1.0 \text{ mol} \cdot \text{L}^{-1}$ ,  $13.7 \text{ mL} \cdot \text{min}^{-1}$ ), a sodium aluminate solution (basic reactant,  $3.0 \text{ mol} \cdot \text{L}^{-1}$ ,  $18.0 \text{ mL} \cdot \text{min}^{-1}$ ) and additional water ( $46.1 \text{ mL} \cdot \text{min}^{-1}$ ) over 30 minutes. The molar ratio  $R_{b/a}$  (defined as the molar ratio of  $\text{NaAl}(\text{OH})_4$  over  $\text{Al}_2(\text{SO}_4)_3$ ) was 4.0, and both temperature and pH value of the suspension were controlled at  $60 \text{ }^\circ\text{C}$  and 9.7, respectively. After the synthesis, the suspension was filtered and washed five times using hot water in order to minimize the impurities content ( $\text{Na}^+$  and  $\text{SO}_4^{2-}$ ). Then, the filtration cake was dried at  $120 \text{ }^\circ\text{C}$  overnight and ground. The obtained boehmite dried precursor was labeled as B.

### 2.2 Synthesis of AACH

Reagent grade aluminium nitrate (Alfa Aesar) and carbonate ammonium (Alfa Aesar) were used as starting materials without further purification.

The synthesis was carried out in a stirred tank reactor equipped with a mechanical stirrer (Figure 1) and containing an initial 667 mL water volume. AACH was precipitated by simultaneous dosing of an aluminium nitrate solution (acid reactant, 1.2 mol.L<sup>-1</sup>, 21.8 mL.min<sup>-1</sup>), a carbonate ammonium solution (basic reactant, 2.0 mol.L<sup>-1</sup>, 39.3 mL.min<sup>-1</sup>) over 30 minutes. The molar ratio  $R_{b/a}$  (defined as the molar ratio of (NH<sub>4</sub>)<sub>2</sub>CO<sub>3</sub> over Al(NO<sub>3</sub>)<sub>3</sub>) was 3.0, and the suspension temperature was controlled at 60 °C. pH was monitored between 7 and 8. After synthesis, the suspension was filtered and washed once with hot water. Then the cake was dried at 120 °C overnight and ground. The obtained AACH dried precursor was labeled as A.

### 2.3 Preparation of Al<sub>2</sub>O<sub>3</sub>

Dried boehmite and AACH were calcined in static air in a muffle furnace at 500, 700 or 1000 °C for 4 h, using a ramp of 2 °C.min<sup>-1</sup>. The alumina obtained from precursors B and A were labeled as B-X and A-X, respectively, with X the calcination temperature.

The repeatability of materials preparation was checked: boehmite and AACH precipitations, and the subsequent calcinations, were performed between 3 and 5 times. The analysis (see section 2.4) shows relative variations of 6% and 11% for the specific area and pore volumes, respectively, of alumina and 3% for the crystallite sizes of boehmite and AACH.

### 2.4 Characterization methods

The crystal phase identification was done by powder X-ray diffraction (XRD). Data were collected on a PANalytical X'Pert Pro  $\theta$ - $\theta$  diffractometer in Bragg-Brentano geometry, using filtered Cu K $\alpha$  radiation and a graphite secondary-beam monochromator. Diffraction intensities were measured, at room temperature, by scanning from 5 to 72° with a step size of 0.033° (2 $\theta$ ). Crystallite sizes were determined using Scherrer's equation.

The nitrogen adsorption-desorption isotherms were collected at 77 K using an adsorption analyzer Micromeritics ASAP 2420. Boehmite, AACH and Al<sub>2</sub>O<sub>3</sub> samples were previously degassed in vacuum for 3 h at 250 °C, 6 h at 80 °C and 6 h at 150 °C, respectively. The specific surface area ( $S_{BET}$ ) was determined by the BET method in pressure domain  $0.05 \leq P/P_0 \leq 0.35$ , and t-plot method was used to evaluate microporosity. Pore size distributions (PSD) were calculated from the desorption branches of the isotherms using the BJH model. The mean pore diameter ( $D_p$ ) corresponds to the maximum of the pore size distribution. When the PSD is not monomodal, we report two (or more)  $D_p$  values corresponding to the two (or more) observed local maxima. Pore volume ( $V_p$ ) was calculated from the adsorbed volume of gas,  $V_{ads}$  at the higher relative pressure ( $P/P_0 \approx 0.99$ ).

Transmission electron microscopy (TEM) observations were performed on a Tecnai microscope (FEI) with accelerative voltage of 200 kV and equipped with HAADF-STEM and EDX detectors. A small amount of powder was dispersed in alcohol using an ultrasound bath. Then a droplet was deposited on a carbon-coated grid and dried under a UV lamp.

Thermogravimetric analysis (TGA) was conducted on a thermogravimetric analyzer STA 449 C (NETZSCH), under air atmosphere with a heating rate of 10 °C.min<sup>-1</sup>. The thermogravimetric analyzer was equipped with a QMS 403 C mass spectrometer.

Fourier transform infrared (FTIR) spectroscopy was carried out in a Bruker Vertex702 spectrometer equipped with a MCT detector (transmission mode). 128 scans with a resolution of 4 cm<sup>-1</sup> were collected. The sample was pretreated at 80 °C during 5h30 under medium vacuum.

## 3. Results and discussion

### 3.1 Protocol adaptation to pure AACH preparation

#### 3.1.1 Solid phase concentration and molar ratio

Both boehmite and AACH were precipitated in such conditions that the final suspension contained approximately the same concentration of solid phase (42-44 g.L<sup>-1</sup>). For AACH synthesis, this implied that precipitation has to be carried out using a low  $R_{b/a}$  molar ratio. In such conditions, the choice of an appropriate precipitating agent is crucial to get pure AACH: ammonium carbonate was preferred to ammonium hydrogen

carbonate, as the latter generally lead to a more or less significant formation of boehmite [11,18,22]. In addition, it should be noted that despite a similar concentration of solid phase in the tested protocols for both precursors, aluminium content was lower in AACH one, which means a lower alumina concentration. Indeed, higher alumina concentration levels can generally be reached with boehmite precipitation pathway as both reactants can bring aluminium ions.

The sensitivity of the suspension pH to the molar ratio appeared to be very different, following the boehmite protocol or the AACH protocol. In boehmite case, a slight variation of the molar ratio  $R_{b/a}$  between 3 and 4 induced a strong variation of the pH value in the range of 5 to 10. On the contrary, we observed in AACH case that a strong variation of the molar ratio  $R_{b/a}$  between 3 and 11 induced a slight variation of the pH value in the range of 7 to 8 (Figure S1). This difference of behaviour is due to the buffer effect of the  $(\text{NH}_4)_2\text{CO}_3$  solution (pH=8.5 at 50 °C) used as basic reactant for AACH preparation (on contrary, the other aqueous solutions of aluminum salts have no buffer effect). As a consequence, AACH precipitation conditions turned out to be less sensitive to this synthesis parameter. A better control of the precursor properties can thus be expected.

### 3.1.2 Optimization of the filtration / washing step

When filtration is carried out at constant pressure, filtrate volume  $V$  can be linked to filtration time  $t$  thanks to the Kozeny-Carman equation [23]:

$$\frac{t}{V} = \frac{\mu R_s W}{2A_f^2 \Delta P} \cdot V + cst$$

where  $\mu$  is the dynamic viscosity ( $\text{Pa}\cdot\text{s}^{-1}$ ),  $W$  is the dry cake mass per unit filtrate volume ( $\text{kg}\cdot\text{m}^{-3}$ ),  $A_f$  is the filtration area ( $\text{m}^2$ ) and  $\Delta P$  the filtration differential pressure (Pa).  $R_s$  is the specific resistance of the filter cake ( $\text{m}\cdot\text{kg}^{-1}$ ) and represents the filterability of a suspension, regardless of the operating conditions if assuming an incompressible cake (ideal case). Both boehmite and AACH specific resistance were estimated experimentally by measurements of filtrate volumes obtained as a function of time (Table 1). In the studied conditions, boehmite suspension thus exhibited a much better filterability than AACH suspension. In practice, this involved filtration times of less than a minute for boehmite suspension, and more than an hour for AACH suspension.

The cake washing is an important step in the preparation of a catalyst support, which aims to remove parasite phases, generally due to the reaction by-products. In boehmite preparation, this step also aims to remove adsorbed  $\text{Na}^+$  and  $\text{SO}_4^{2-}$  counter-ions which could negatively impact its textural properties or poison the active sites on the final catalyst. Several washing were necessary, leading to a final washing volume over suspension volume ratio ( $V_{\text{washing}}/V_{\text{suspension}}$ ) in the order of 5. One of AACH interests is its ability to give high purity alumina, as the majority of ions involved in the synthesis are easily degraded and evacuated during calcination step. However, in the absence of washing, ammonium nitrate traces were observed by XRD (Figure 2). A washing step is thus necessary to get pure AACH.

Washing influence on AACH cake was studied by carrying out several unit washing until reaching a final  $V_{\text{washing}}/V_{\text{suspension}}$  ratio of 3.2. After each unit washing, cake and filtrate samples were collected. The first was dried and analyzed by XRD to determine the crystallized phase composition. The latter was analyzed by ionic chromatography to measure the change in nitrate ions content. The experiment results showed a rapid decrease in the nitrate content in the filtrate from the first washing ( $V_{\text{washing}}/V_{\text{suspension}} = 0.4$ ) (Figure 3). This trend was confirmed by the disappearance of the crystallized ammonium nitrate phase observed in the cake before the first washing (Figure 2). However, we also observed that excessive washing ( $V_{\text{washing}}/V_{\text{suspension}} > 1.6$ ) could lead to a progressive formation of boehmite phase, while crystallized AACH was disappearing. This was consistent with the findings of Stoica et al. [20] about the highly reactive nature of AACH in deionized water. In our case, such a transformation was possible because of the poor filterability of AACH suspension and therefore the long time during which the cake was exposed to water. According to this study, the  $V_{\text{washing}}/V_{\text{suspension}}$  ratio was set at 0.5, in order to remove crystallized ammonium nitrate and avoid a transformation from AACH to boehmite. It is interesting to note that this ratio is ten times lower than that of boehmite.

### 3.2 As-synthesized materials

Figure 4 shows the XRD patterns of the two synthesized precursors. As expected from the optimized preparation protocols, only one phase was identified in each sample: boehmite (JCPDS-ICDD 21-1307) in B and AACH (JCPDS-ICDD 42-0250) in A. Table 2 shows both boehmite and AACH crystallite sizes for different planes. The sizes were calculated from XRD using Scherrer's equation. This calculation assumes that XRD peak broadening observed for these nanoparticles is mainly due to size and shape effect and that strain effect can be neglected. This assumption has been demonstrated for boehmite nanoparticles [24] and is also probably true for AACH nanoparticles.

Boehmite sample B exhibited small crystallites sizes below 5 nm. This estimation from XRD was consistent with the transmission electron microscopy observations as it evidenced the presence of nanoparticles in this size domain (Figure 5b). This observation is consistent with that the chosen precipitation operating conditions (pH=9.7 close to minimum Al solubility, T=60 °C, high Al concentration) favor high nucleation rates and leads to small nanoparticles. On a larger scale, we also observed that the crystallites seemed to aggregate to form very thin plate-like secondary particles (Figure 5a). Their length ranged from 20 to 120 nm, while their thickness was of the same order of magnitude as for boehmite crystallites. Once more, high temperature, high particles concentration and pH value close the boehmite PZC favor strong aggregation. Formation of such fibrous particles has already been observed in literature by TEM [25,26] and can be explained by crystallites oriented aggregation, a common phenomenon for boehmite [24]. It has been recently proposed that sulfate anions absorbed on boehmite play a key role for this oriented aggregation [27].

AACH sample A exhibited crystallites in the size range of 10-20 nm. This estimation from XRD appeared to be two to four times smaller than the size of individual particles observed by transmission electron microscopy (Figure 5c and d). An explanation for this size difference could be that the observed particles were small aggregates of crystallites that fused under the high energy TEM electron beam, as AACH was noticed to be even more sensitive to it than boehmite. Additionally, for both boehmite and AACH samples, higher resolution TEM and SAED analysis cannot be performed, since the electron beam induces particles sintering and amorphisation.

The FTIR spectrum of B (Figure 6) exhibits the characteristic features of AACH structures. The vibrational bands of hydroxyl, ammonium and carbonate groups can be found: OH<sup>-</sup> (3435, 997 cm<sup>-1</sup>), NH<sub>4</sub><sup>+</sup> (3172, 3005, 2854, 1836, 1720 cm<sup>-1</sup>) and CO<sub>3</sub><sup>2-</sup> (1576, 1456, 1388, 1109 cm<sup>-1</sup>). The spectrum is similar to published ones [28], except the band at 1317 cm<sup>-1</sup> that was not previously observed, the larger bands broadening and different relative intensities: these features are probably due to the small crystallites size of AACH particles (see XRD analysis before).

Figure 7a gives the N<sub>2</sub> isotherms of the synthesized precursors. According to IUPAC classification, B sample exhibited a combination of type II and IV isotherms while A sample exhibited a type IV isotherm. Both precursors thus had characteristics of mesoporous materials, but differences in their hysteresis loop can be observed. It can be interpreted as a difference in both their pore shape and pore size distribution, which can be related to the different morphologies and arrangements of their respective nanoparticles.

The textural properties of B and A samples are listed in Table 3. Boehmite sample exhibited a high specific surface area near 300 m<sup>2</sup>.g<sup>-1</sup> due to a narrow pore size distribution centered around 4 nm (Figure 7b). In comparison, AACH sample exhibited a specific surface area twice as small (148 m<sup>2</sup>.g<sup>-1</sup>) but a higher porosity. In particular, the mean pore diameter was almost nine times higher and the pore size distribution was broader. It is interesting to note that mean pore diameters of both precursors were consistent with the crystallite sizes estimated using Scherrer's equation. Moreover, almost no microporosity was detected.

### 3.3 Calcined materials

#### 3.3.1 Precursor – alumina transition

The thermal transformation process of boehmite and AACH to  $\gamma$ -Al<sub>2</sub>O<sub>3</sub> was characterized by TGA (see the Supporting Information, Figure S2). As expected, sample B exhibited two endothermic peaks, characteristic of boehmite behavior [5]. These peaks are located around 100 °C and 400 °C, and correspond respectively to the desorption of the physisorbed water and to the precursor dehydroxylation (transition into  $\gamma$ -alumina). The total mass loss of B was 26%. This value is above the theoretical 15%, which confirms the presence of physisorbed water in addition with chemisorbed water. Sample A exhibited a single sharp endothermic peak around 200 °C, which correlate with a strong mass loss (50%). This peak is characteristic of AACH and corresponds to the simultaneous release of CO<sub>2</sub>, NH<sub>3</sub> and H<sub>2</sub>O [29]. The final mass loss measured on A samples was 60%. The small difference with the theoretical mass loss (63%) can be attributed to the presence of amorphous Al-containing phase(s) [9,28]. Once again, it is important to note that since AACH mass loss during calcination is higher than boehmite ones, less AACH-derived alumina will be obtained for a same solid concentration in the final suspension.

Boehmite and AACH precursors were calcined at 500 °C. N<sub>2</sub> isotherms of the calcined materials were measured immediately after the calcination step to evaluate their textural properties (Table 4). The textural properties evolution turned out to be very different according to the precursor considered.

In boehmite case, transition into  $\gamma$ -alumina led to a slight increase of pore diameter (Figure 8) and a 20% increase of pore volume, but did not seem to affect the specific surface area, which remained around 300 m<sup>2</sup>.g<sup>-1</sup>. Boehmite transformation is topotactic [30], which means that particles morphological characteristics are broadly conserved during the phase transition. As a consequence, the textural properties of boehmite-derived alumina are strongly conditioned by that of boehmite precursor. Thermal treatment thus leads to the collapse of the boehmite lamellar structure and to crystallite volume contraction. This is consistent with the observed increase in both pore volume and mean pore diameter, from 0.70 to 0.83 cm<sup>3</sup>.g<sup>-1</sup> and from 3.9 to 5.6 nm, respectively. The mass loss during the calcinations leads to a decrease in the specific surface area, which is nonetheless compensated by the material densification. That is why the alumina specific surface area was in the same range as that of its precursor.

In AACH case, an important rise of pore volume (40%) was noted, while the specific surface area increased dramatically to exceed 400 m<sup>2</sup>.g<sup>-1</sup>. A slight variation was also observed on the mean pore diameter, but given the broad pore size distribution, it was not thought to be particularly significant (Figure 8). Overall, AACH transition into  $\gamma$ -alumina led to a more pronounced evolution of the textural properties than boehmite transition. In the literature, this strong evolution is usually related to the simultaneous removal of CO<sub>2</sub>, NH<sub>3</sub> and H<sub>2</sub>O [12,18]. Hu et al. [15] suggested that the release of these gas results in the cracking of the AACH crystallites and the formation of an intracrystalline porosity. As a consequence, this would lead to an increase in the disorder level of the crystallographic structure of AACH-derived alumina. This statement was substantiated comparing both XRD patterns of boehmite-derived and AACH-derived  $\gamma$ -aluminas (Figure 9), in which the latter showed poorer crystalline definition.

It can be noticed that AACH-derived alumina exhibited a secondary pore distribution in the range 2 to 5 nm, and probably below. The reliability of the BJH desorption branch in this size area is controversial, as artificial peaks can appear (generally around 4 nm) due to spontaneous evaporation of metastable pore liquid, and as a matter of fact are not associated with a real group of pores. However, the PSD derived from the BJH adsorption branch is free from this artifact [31]. In our case, both BJH adsorption and desorption branches exhibited this secondary population (see the Supporting Information, Figure S3), suggesting that it is not an artifact. Considering that this secondary population was not observed on AACH precursor, we assumed that this new porosity originated from AACH thermal decomposition process, as discussed previously. This assumption was supported by TEM image of A-500 (Figure 10), where intracrystalline porosity in the size range 1-5 nm could be observed. Moreover, application of the t-plot method revealed that more than 50 % of the specific surface area of AACH-derived alumina was due to microporosity. So we can reasonably assume that calcination step of AACH led to the formation of an intracrystalline secondary pore population, distributed around the limit between micro- and mesoporosity, which explained the strong increase in the specific surface area. Such a bimodal porous structure has already been reported in previous works [15,32], even though its formation was not always discussed.

However, formation of such an intracrystalline porosity is not sufficient to explain the strong increase observed in pore volume. Besides, this increase seemed not to be linked to a broadening of the pore size, but to an increase in the already existing pore population density. A hypothesis could be that gas removal has permitted the access to closed pores.

Finally, AACH led to a more porous alumina, with mean pore diameter five times larger than that of boehmite-derived alumina. However, due to the high level of microporosity observed on AACH-derived alumina, only part of its high specific surface area would be useful in refining processes.

### 3.3.2 Thermal evolution of boehmite-derived and AACH-derived aluminas

Boehmite-derived and AACH-derived aluminas were compared on the basis of their textural properties evolution between 500 °C and 1000 °C (Table 4). After calcinations at 700 °C, a decrease in the specific surface area was observed, both aluminas exhibiting values close to 240 m<sup>2</sup>.g<sup>-1</sup>. This drop was particularly pronounced for AACH-derived alumina and was related to a strong decrease in microporosity. Concerning the porosity evolution, two different trends were noticed. On boehmite-derived alumina, the temperature increase led to an increase in the mean pore diameter but had no effect on the pore volume. On the contrary, on AACH-derived alumina, no variation of the mean pore diameter was observed, but the pore volume decreased. The secondary pore population ( $D_p < 5$  nm) was also much less significant than at 500 °C (Figure 8). After calcinations at 1000 °C, specific surface areas were equally impacted, dropping to about 110 m<sup>2</sup>.g<sup>-1</sup>. Almost no microporosity was detected in both aluminas at that point. Concerning the porosity evolution, the trend remained to some extent the same compared with the observations at 700 °C, except a slight pore volume decrease on the boehmite-derived alumina. It was also noted that the secondary pore population entirely disappeared at this temperature (Figure 8).

Taking into account the above observations, it seems that boehmite-derived and AACH-derived aluminas do not exhibit the same behavior against sintering. In boehmite-derived alumina case, thermal evolution of the textural properties is well documented in the literature [1]. Sintering leads to an increase in the crystallite size with calcinations temperature. That explains the significant broadening of the mean pore diameter, from about 6 nm at 500 °C to more than 14 nm at 1000 °C, as well as its pore size distribution (Figure 8 and Figure 11). This leads to a progressive decrease in the specific surface area, which is more significant between 700 °C and 1000 °C because of the change in the crystallographic structure. In return, the mean pore diameter broadening allows the conservation of a constant pore volume between 500 °C and 700 °C ( $V_p = 0.82$  cm<sup>3</sup>.g<sup>-1</sup>) and limits its contraction even at 1000 °C ( $V_p = 0.74$  cm<sup>3</sup>.g<sup>-1</sup>), except a progressive densification of the material (Figure 12a). Sintering of boehmite-derived alumina can thus be considered as a broadly constant pore volume phenomenon in the temperature range 500 °C to 1000 °C, during which only mean pore diameter and specific surface area evolve.

On the contrary, for AACH-derived alumina case, it seems that sintering occurs at constant mean pore diameter in the temperature range 500 °C to 1000 °C, while pore volume and specific surface area evolve. Moreover, textural properties evolution appears to be a two-step process.

In a first step, between 500 °C and 700 °C, a strong decrease in microporosity and in the secondary pore population was observed (Figure 8). A possible explanation could be that the cracked crystallites were particularly subject to sintering, leading to the elimination of intracrystalline porosity. The sintering phenomenon, particularly promoted on the small particles, thus enabled “repair” of the cracked crystallites, but no further growth, which is consistent with the constant mean pore diameter. Figure 13 shows a schematic representation of this supposed process. Disappearance of intracrystalline porosity was also consistent with the drop of the specific surface area: this is due to the strong decrease in microporosity, while the mesoporous surface area remained the same (Figure 12b). In the same way, the decrease in pore volume between 500 °C and 700 °C could mostly be related to the intracrystalline porosity disappearance (Figure 12a).

In a second step, between 700 °C and 1000 °C, the main mean pore diameter remained stable, but the pore size distribution tightened, in particular in the small pore diameters domain (Figure 8), probably because of a stronger sintering. As a consequence, both mesoporous surface area and pore volume decreased (Figure 12).

AACH-derived alumina thus distinguished itself from boehmite-derived alumina by its ability to maintain a constant mean pore diameter, regardless of the calcinations temperature. It might nonetheless be questioned whether this atypical property is only due to the large pore diameters of the material, hardly impacted by sintering, or is specific to AACH nature. In our opinion, the latter assumption seems to be the most probable as a same tendency to the conservation of a constant mean pore diameter was observed on other AACH-derived aluminas exhibiting mean pore diameter between 10 and 15 nm (data not shown here).

#### 4. Conclusions

In this work, pure boehmite and AACH were precipitated in the same stirred tank reactor with closest as possible process precipitation parameters (concentration, pH, duration ...) and similar post-treatment conditions (washing, drying, calcination ...). Boehmite and AACH are two possible precursors to prepare porous  $\gamma$ -alumina with high porosity, suitable for catalytic applications: using this methodology, for the two materials, we had compared in a consistent way the preparation advantages / disadvantages, as well as the porosity of the obtained  $\gamma$ -alumina.

Comparison of both preparation protocols led to the following observations that help for the choice of an appropriate preparation route for alumina precursor synthesis:

- The use of ammonium carbonate as precipitating agent was confirmed to allow the formation of pure AACH even at low  $R_{b/a}$  molar ratio,
- At identical solid phase concentration in the final suspension, the boehmite route led to a higher content of alumina,
- AACH suspension pH was less sensitive to small variations of the synthesis parameters than that of boehmite, leading to a better control of the solid properties,
- A significant reduction of the washing water volume was achieved with AACH route compared to boehmite route.

Beyond that, evolution of the textural properties of boehmite-derived and AACH-derived aluminas at different temperature was compared. The proposed AACH route allowed the obtention of alumina with original textural properties compared with boehmite route. In particular, AACH-derived alumina exhibited a high porosity, with a mean pore diameter five-time larger than boehmite-derived alumina at 500 °C. However, the high increase in specific surface area usually reported in the literature was attributed here to the formation of microporosity due to the particular AACH-alumina transition mechanism. Nonetheless, it was also observed that AACH-derived alumina exhibited an atypical behavior against sintering, in particular through keeping a constant mean pore diameter, regardless of the calcinations temperature. This promising material could thus be used between 500 °C and 700 °C with constant mean pore diameter and mesoporous surface area, while exhibiting a higher pore volume than boehmite-derived alumina.

#### Acknowledgements

The authors would like to thank the Physics and Analysis Division (IFPEN) for technical assistance, especially Laurent Lemaitre.

This research did not receive any specific grant from funding agencies in the public, commercial, or not-for-profit sectors.

#### References

- [1] P. Euzen, P. Raybaud, X. Krokidis, H. Toulhoat, J.-L. Le Loarer, J.-P. Jolivet, et al., Alumina, in: F. Schüth, K.S.W. Sing, J. Weitkamp (Eds.), *Handb. Porous Solids*, Wiley-VCH, Weinheim, 2002.
- [2] G. Busca, Structural, Surface, and Catalytic Properties of Aluminas, in: *Adv. Catal.* Vol. 57, Elsevier B.V., 2014: pp. 319–404. doi:10.1016/B978-0-12-800127-1.00003-5.
- [3] M. Trueba, S.P. Trasatti,  $\gamma$ -Alumina as a Support for Catalysts: A Review of Fundamental Aspects, *Eur. J. Inorg. Chem.* 2005 (2005) 3393–3403. doi:10.1002/ejic.200500348.
- [4] D. Papée, R. Tertian, R. Biais, Recherches sur la constitution des gels et des hydrates

- cristallisés d'alumine, *Bull. Soc. Chim. Fr.* 5 (1958) 1301–1310.
- [5] P. Alphonse, M. Courty, Structure and thermal behavior of nanocrystalline boehmite, *Thermochim. Acta.* 425 (2005) 75–89. doi:10.1016/j.tca.2004.06.009.
- [6] K.P. Prodromou, A.S. Pavlatou-Ve, Formation of Aluminum Hydroxides as Influenced by Aluminum Salts and Bases, *Clays Clay Miner.* 43 (1995) 111–115. doi:10.1346/CCMN.1995.0430113.
- [7] J. Čejka, Organized mesoporous alumina: synthesis, structure and potential in catalysis, *Appl. Catal. A Gen.* 254 (2003) 327–338. doi:10.1016/S0926-860X(03)00478-2.
- [8] A.A. Ali, M.A. Hasan, M.I. Zaki, Dawsonite-Type Precursors for Catalytic Al, Cr, and Fe Oxides: Synthesis and Characterization, *Chem. Mater.* 17 (2005) 6797–6804. doi:10.1021/cm0519131.
- [9] R.F. Vogel, G. Marcelin, W.L. Kehl, The preparation of controlled pore alumina, *Appl. Catal.* 12 (1984) 237–248. doi:10.1016/S0166-9834(00)80294-8.
- [10] I. Pitsch, W. Geßner, A. Brückner, H. Mehner, S. Möhmel, D.-C. Uecker, et al., Synthesis and characterization of Fe<sub>2</sub>O<sub>3</sub> containing aluminas by thermal decomposition of modified ammonium dawsonite, *J. Mater. Chem.* 11 (2001) 2498–2503. doi:10.1039/b101466h.
- [11] D.-C. Shin, S.S. Park, J.H. Kim, S.S. Hong, J.M. Park, S.H. Lee, et al., Study on  $\alpha$ -alumina precursors prepared using different ammonium salt precipitants, *J. Ind. Eng. Chem.* 20 (2014) 1269–1275. doi:10.1016/j.jiec.2013.07.003.
- [12] C.-C. Ma, X.-X. Zhou, X. Xu, T. Zhu, Synthesis and thermal decomposition of ammonium aluminum carbonate hydroxide (AACH), *Mater. Chem. Phys.* 72 (2001) 374–379. doi:10.1016/S0254-0584(01)00313-3.
- [13] M. Santiago, M.S. Yalfani, J. Pérez-Ramírez, In-line dispersion-precipitation method for the synthesis of metal-substituted dawsonites. Genesis of oxide materials with superior properties, *J. Mater. Chem.* 16 (2006) 2886. doi:10.1039/b607031k.
- [14] D.C. Dubert, J. Pérez-Ramírez, R. Garcia-Valls, Continuous Synthesis of Porous Ammonium Dawsonite Within a New Microstructured System, *Chem. Eng. Trans.* 25 (2011) 231–236. doi:10.3303/CET1125039.
- [15] X. Hu, Y. Liu, Z. Tang, G. Li, R. Zhao, C. Liu, Fabrication of high-surface-area  $\gamma$ -alumina by thermal decomposition of AACH precursor using low-temperature solid-state reaction, *Mater. Res. Bull.* 47 (2012) 4271–4277. doi:10.1016/j.materresbull.2012.09.019.
- [16] H. Liu, H. Sun, J. Li, X. He, Z. Zhu, pH-dependent formation of AACH fibers with tunable diameters and their in situ transformation to alumina nanocrystals with mesoporous structure, *Adv. Powder Technol.* 23 (2012) 164–169. doi:10.1016/j.apt.2011.01.008.
- [17] C. Liu, J. Li, K. Liew, J. Zhu, M.R. bin Nordin, An environmentally friendly method for the synthesis of nano-alumina with controllable morphologies, *RSC Adv.* 2 (2012) 8352. doi:10.1039/c2ra20674a.
- [18] G.-C. Li, Y.-Q. Liu, L.-L. Guan, X.-F. Hu, C.-G. Liu, Meso/macroporous  $\gamma$ -Al<sub>2</sub>O<sub>3</sub> fabricated by thermal decomposition of nanorods ammonium aluminium carbonate hydroxide, *Mater. Res. Bull.* 47 (2012) 1073–1079. doi:10.1016/j.materresbull.2011.12.026.
- [19] X. Duan, T. Kim, D. Li, J. Ma, W. Zheng, Understanding the effect models of ionic liquids in the synthesis of NH<sub>4</sub>-Dw and  $\gamma$ -AlOOH nanostructures and their conversion into porous  $\gamma$ -Al<sub>2</sub>O<sub>3</sub>., *Chemistry.* 19 (2013) 5924–37. doi:10.1002/chem.201203176.
- [20] G. Stoica, J. Pérez-Ramírez, Stability and inter-conversion of synthetic dawsonites in aqueous media, *Geochim. Cosmochim. Acta.* 74 (2010) 7048–7058. doi:10.1016/j.gca.2010.09.013.
- [21] E. Morgado, Y.L. Lam, L.F. Nazar, Formation of Peptizable Boehmites by Hydrolysis of Aluminum Nitrate in Aqueous Solution, *J. Colloid Interface Sci.* 188 (1997) 257–269. doi:10.1006/jcis.1997.4780.
- [22] Y. Liu, H. Guo, L. Jia, Z. Ma, Y. Xiao, C. Chen, Fischer-Tropsch synthesis over alumina-supported cobalt-based catalysts: Effect of support variables, *J. Mater. Sci. Chem. Eng.* 2 (2014) 19–27.
- [23] D.G. Dickey, *Filtration*, Reinhold, New-York, 1961.
- [24] D. Chiche, M. Digne, R. Revel, C. Chanéac, J.-P. Jolivet, Accurate Determination of Oxide Nanoparticle Size and Shape Based on X-Ray Powder Pattern Simulation: Application to

- Boehmite AlOOH, *J. Phys. Chem. C*. 112 (2008) 8524–8533. doi:10.1021/jp710664h.
- [25] J.P. Jolivet, C. Froidefond, A. Pottier, C. Chanéac, S. Cassaignon, E. Tronc, P. Euzen, Size tailoring of oxide nanoparticles by precipitation in aqueous medium. A semi-quantitative modelling, *J. Mater. Chem.* 14 (2004) 14, 3281-3288. doi:10.1039/B407086K
- [26] F. Karouia, M. Boualleg, M. Digne, P. Alphonse, Control of the textural properties of nanocrystalline boehmite ( $\gamma$ -AlOOH) regarding its peptization ability, *Powder Technol.* 237 (2013) 602–609. doi: 10.1016/j.powtec.2012.12.054
- [27] Y. Xia, L. Zhan, X. Jiao, D. Chen, Synthesis of  $\gamma$ -AlOOH nanocrystals with different morphologies due to the effect of sulfate ions and the corresponding formation mechanism study, *Phys. Chem. Chem. Phys.* 15 (2013) 18290-18299. doi:10.1039/C3CP53110D
- [28] G. Stoica, J. Pérez-Ramírez, Reforming Dawsonite by Memory Effect of AACH-Derived Aluminas, *Chem. Mater.* 19 (2007) 4783–4790. doi:10.1021/cm071351g.
- [29] M.S. Yalfani, M. Santiago, J. Pérez-Ramírez, In situ studies during thermal activation of dawsonite-type compounds to oxide catalysts, *J. Mater. Chem.* 17 (2007) 1222. doi:10.1039/b615264c.
- [30] B.C. Lippens, Structure and texture of aluminas, (1961).
- [31] S. Lowell, J.E. Shields, M.A. Thomas, M. Thommes, Characterization of Porous Solids and Powders: Surface Area, Pore Size and Density, Kluwer Academic Publisher, Dordrecht, 2004.
- [32] M. Zhang, T. Yang, R. Zhao, C. Liu, Effect of solid-state synthesized alumina properties on the structure and catalytic performance of NiMo catalyst in hydrodesulfurization, *Appl. Catal. A Gen.* 468 (2013) 327–333. doi:10.1016/j.apcata.2013.09.008.

### Nomenclature

$A_f$	Filtration area	$m^2$
$D_p$	Mean pore diameter	nm
$R_s$	Specific resistance of the filter cake	$m.kg^{-1}$
$S_{BET}$	Specific surface area calculated by BET method	$m^2.g^{-1}$
$S_{meso}$	Mesoporous surface area	$m^2.g^{-1}$
$S_{micro}$	Microporous surface area calculated by t-plot method	$m^2.g^{-1}$
$T$	Temperature	$^{\circ}C$
$V_{ads}$	Adsorbed volume of gas	$cm^3$
$V_{micro}$	Microporous volume	$cm^3.g^{-1}$
$V_p$	Pore volume	$cm^3.g^{-1}$
$W$	Cake mass per unit filtrate volume	$kg.m^{-3}$
$\Delta P$	Filtration differential pressure	Pa
$\mu$	Dynamic viscosity	$Pa.s^{-1}$

Figures :

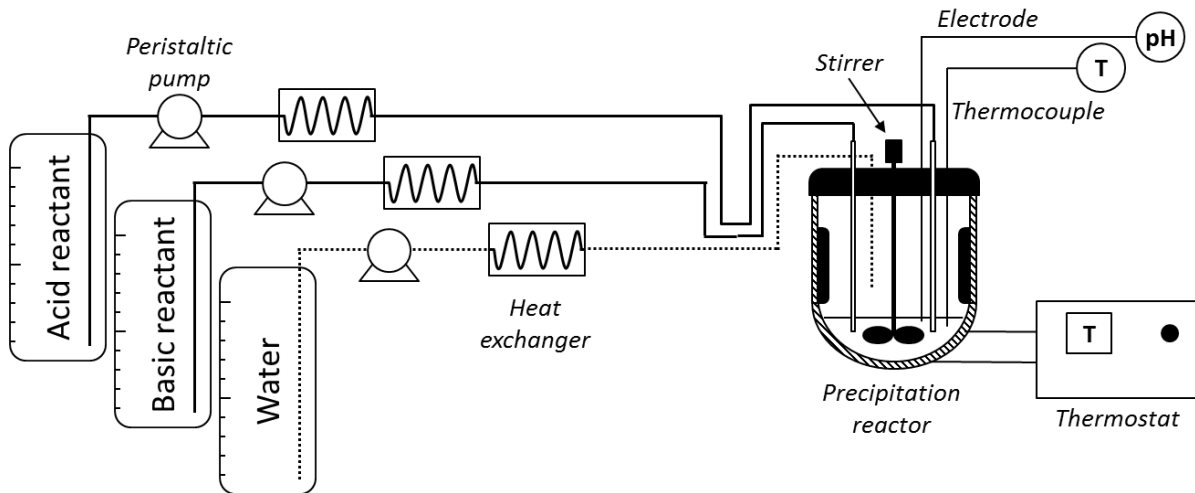


Figure 1. Schematic view of the experimental setup.

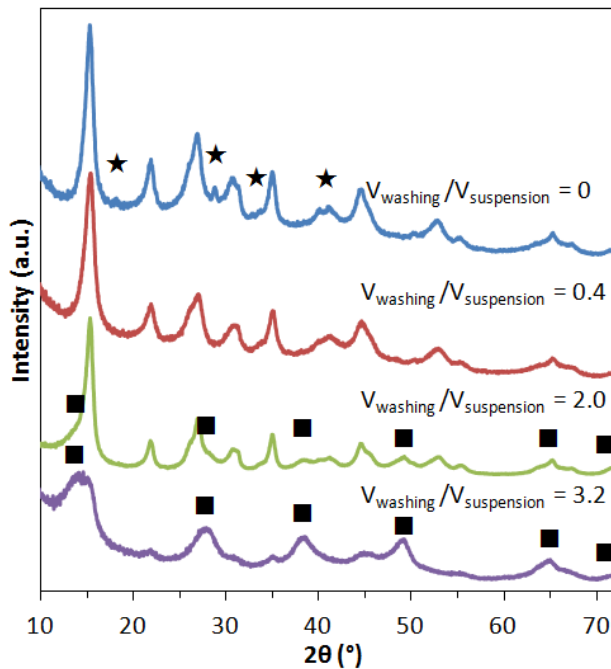


Figure 2. Evolution of the crystallographic phases in AACH cake with increasing washing volumes (secondary phases: ammonium nitrate (★); boehmite (■)).

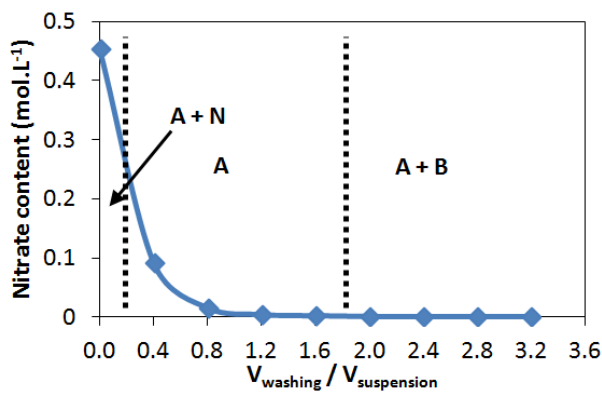
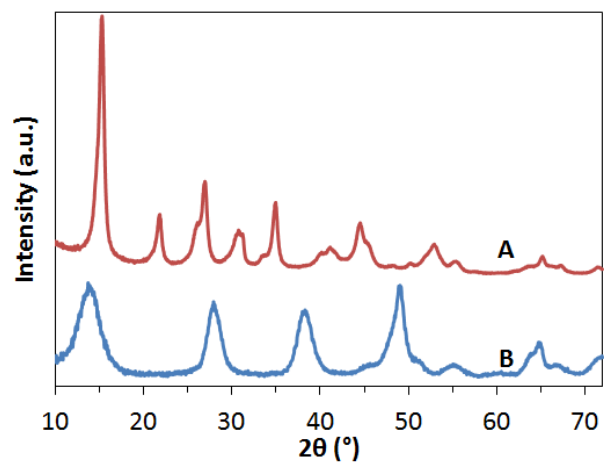
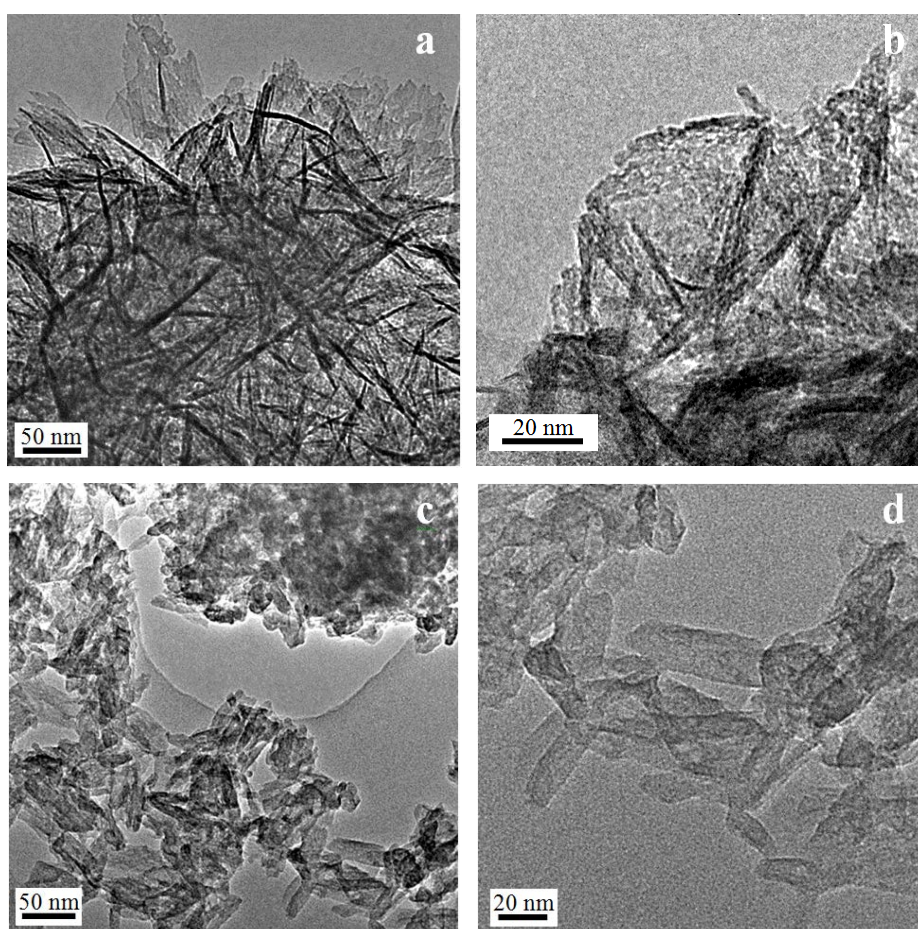


Figure 3. Evolution of nitrate content in the filtrate and crystallized phases in the cake with increasing washing volumes (A: AACH; B: boehmite; N: ammonium nitrate).



**Figure 4.** XRD patterns of the precursors B and A.



**Figure 5.** TEM images of precursors B (a and b) and A (c and d).

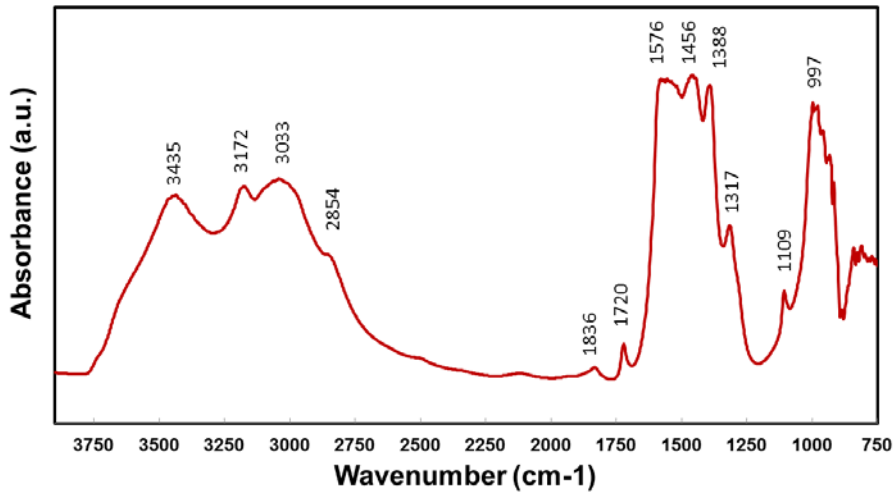


**Figure 6.** FTIR spectrum of the precursor A.

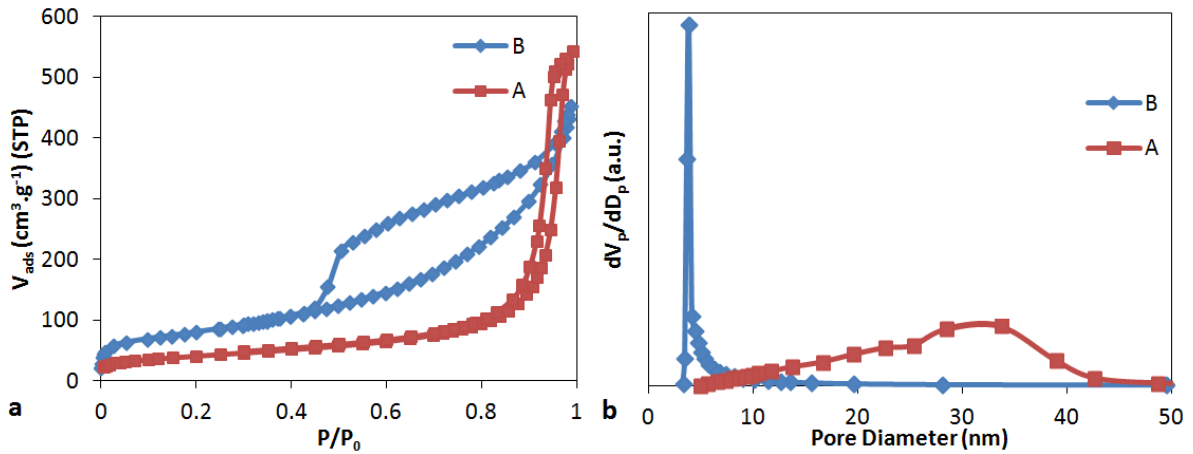


**Figure 7.** (a)  $N_2$  adsorption-desorption isotherms and (b) pore size distributions of boehmite and AACH samples.

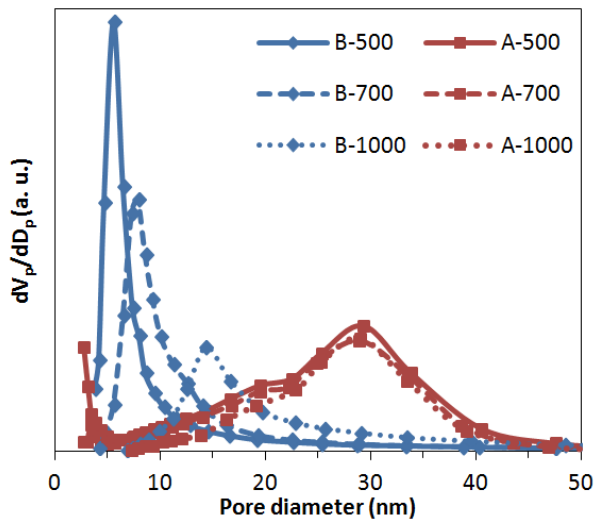


**Figure 8.** Pore size distributions of boehmite-derived and AACH-derived aluminas at different temperatures.

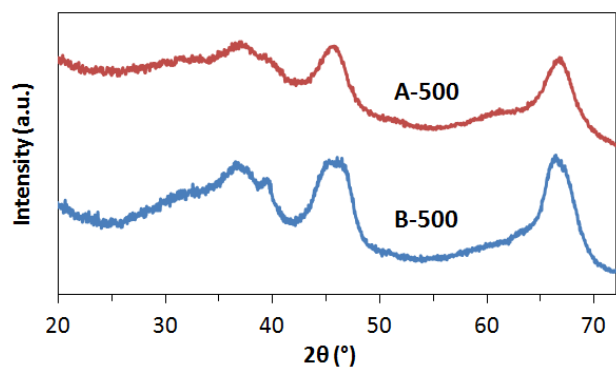


**Figure 9.** XRD patterns of boehmite-derived and AACH-derived  $\gamma$ -aluminas obtained at 500 °C.

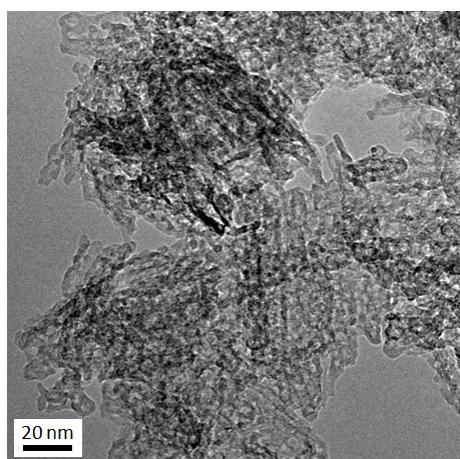


**Figure 10.** TEM image of  $\gamma$ -alumina A-500.

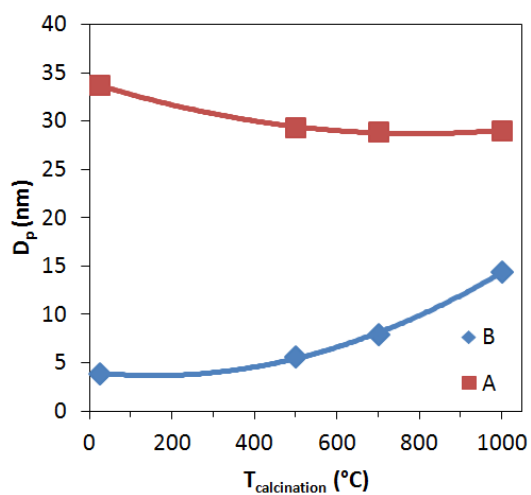


**Figure 11.** Evolution of the mean pore diameter of boehmite-derived and AACH-derived aluminas with temperature.

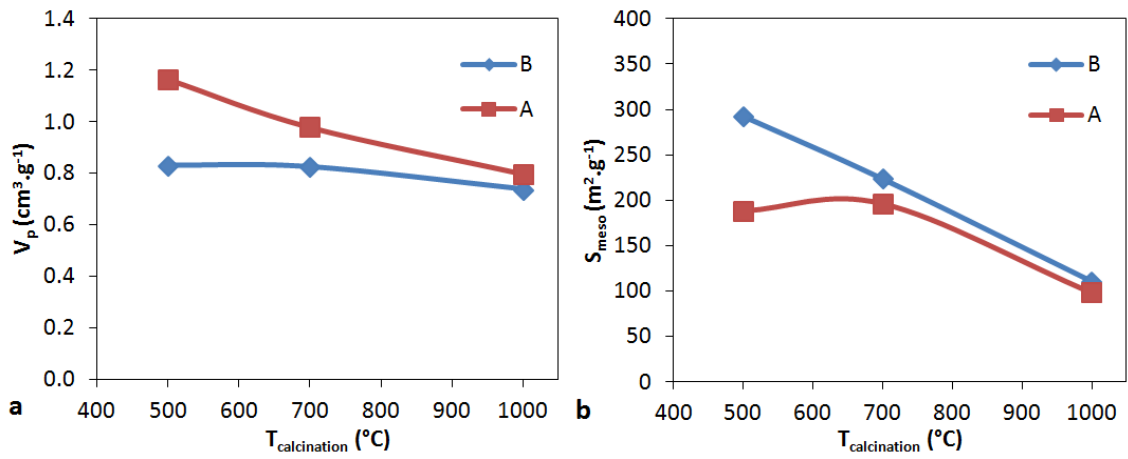


**Figure 12.** Evolution of the pore volume (a) and mesoporous surface area (b) of boehmite-derived and AACH-derived aluminas with temperature.

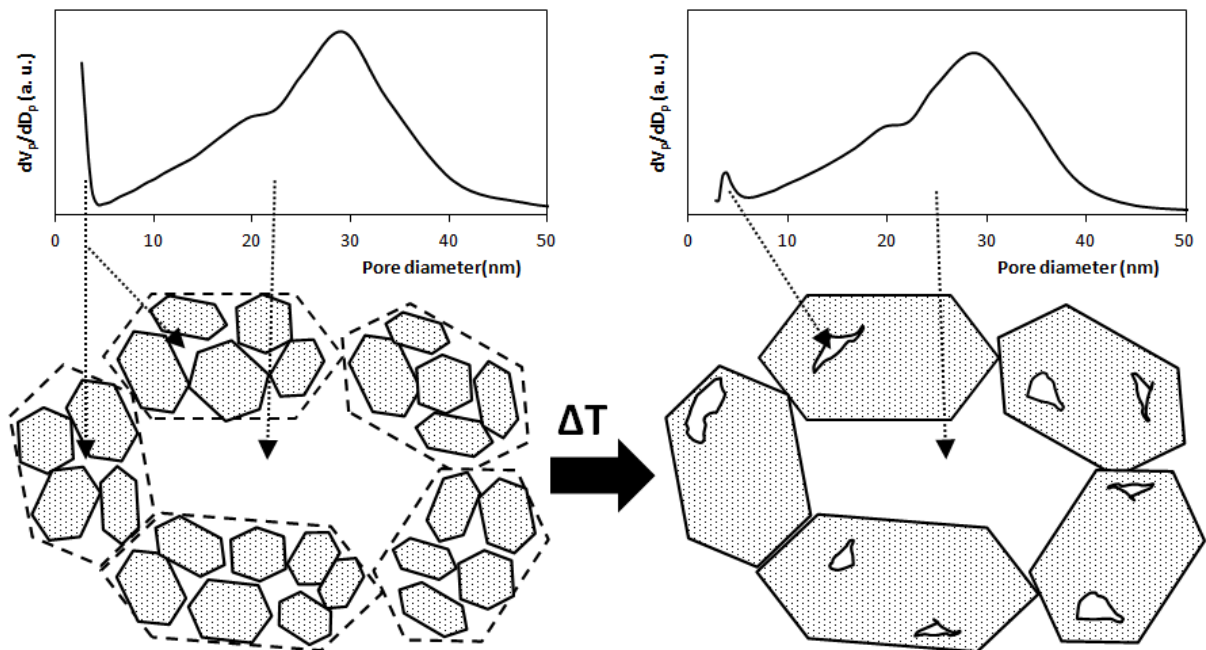


**Figure 13.** Schematic representation of the sintering phenomenon of AACH-derived alumina intracrystalline porosity between 500 °C and 700 °C.

**Tables :****Table 1.** Estimated specific resistance of the filter cake from the studied suspension.

	B suspension	A suspension
$R_s$ (m.kg <sup>-1</sup> )	10 <sup>9</sup>	10 <sup>12</sup>

**Table 2.** Crystallite size according to different crystallographic planes for B and A samples.

Samples	Crystallite size in boehmite phase (nm)		Crystallite size in AACH phase (nm)	
	(020)	(120)	(020)	(111)
B	3.1	4.7	-	-
A	-	-	6.8	16.5

**Table 3.** Textural properties of B and A samples.

Samples	$S_{BET}$ (m <sup>2</sup> .g <sup>-1</sup> )	$S_{micro}$ (m <sup>2</sup> .g <sup>-1</sup> )	$V_p$ (cm <sup>3</sup> .g <sup>-1</sup> )	$V_{micro}$ (cm <sup>3</sup> .g <sup>-1</sup> )	$D_p$ (nm)
B	286	0	0.70	0	3.9
A	148	13	0.84	< 0.01	33.7

**Table 4.** Textural properties of boehmite-derived and AACH-derived aluminas obtained at different temperatures.

Samples	$S_{BET}$ (m <sup>2</sup> .g <sup>-1</sup> )	$S_{micro}$ (m <sup>2</sup> .g <sup>-1</sup> )	$V_p$ (cm <sup>3</sup> .g <sup>-1</sup> )	$V_{micro}$ (cm <sup>3</sup> .g <sup>-1</sup> )	$D_p$ (nm)
B-500	299	7	0.83	0	5.6
B-700	246	23	0.82	0.01	7.9
B-1000	118	8	0.74	0	14.4
A-500	407	219	1.17	0.12	2.7 – 29.3
A-700	241	45	0.98	0.02	3.8 – 28.9
A-1000	107	9	0.80	0	29.0

## Supporting Information

### AACH as an alternative route for alumina preparation: comparison with the classical boehmite precursor

Robin Lafficher<sup>a,b</sup>, Mathieu Digne<sup>a,\*</sup>, Fabien Salvatori<sup>a</sup>, Malika Boualleg<sup>a</sup>, Didier Colson<sup>b</sup> and François Puel<sup>c</sup>

<sup>a</sup> IFP Energies Nouvelles ; BP 3, F-69360 Solaize, France

<sup>b</sup> Univ Lyon, Université Lyon 1, CNRS, UMR5007, LAGEP, F-69622 LYON, France

<sup>c</sup> LGPM, CentraleSupélec, Université Paris-Saclay, F-92295 Châtenay-Malabry, France

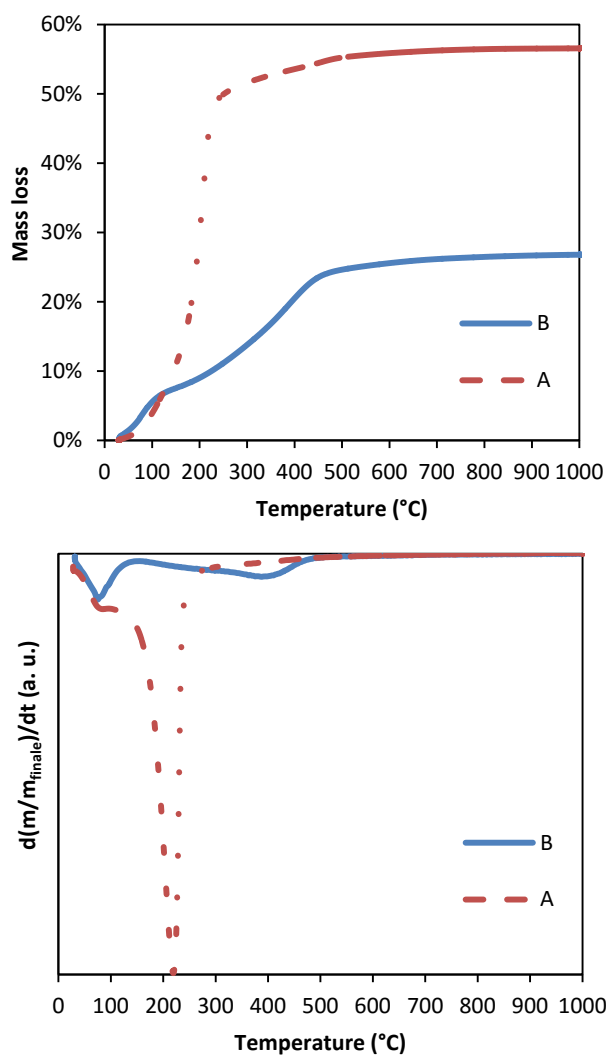


Figure S1. TGA profiles of B and A samples

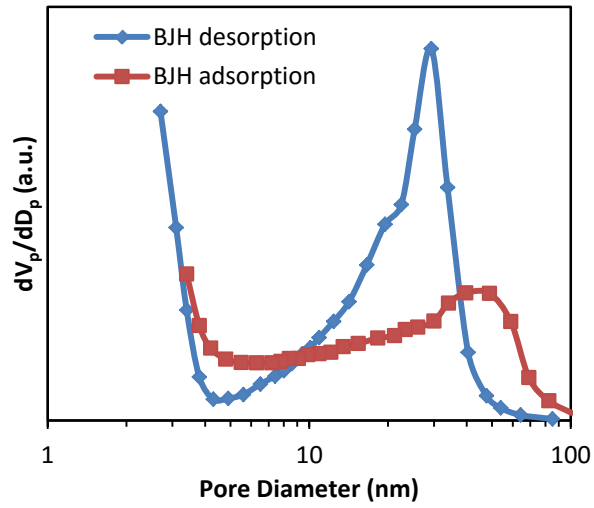


Figure S2. Pore size distribution calculated from the desorption and the adsorption branches of A-500 isotherm using the BJH model

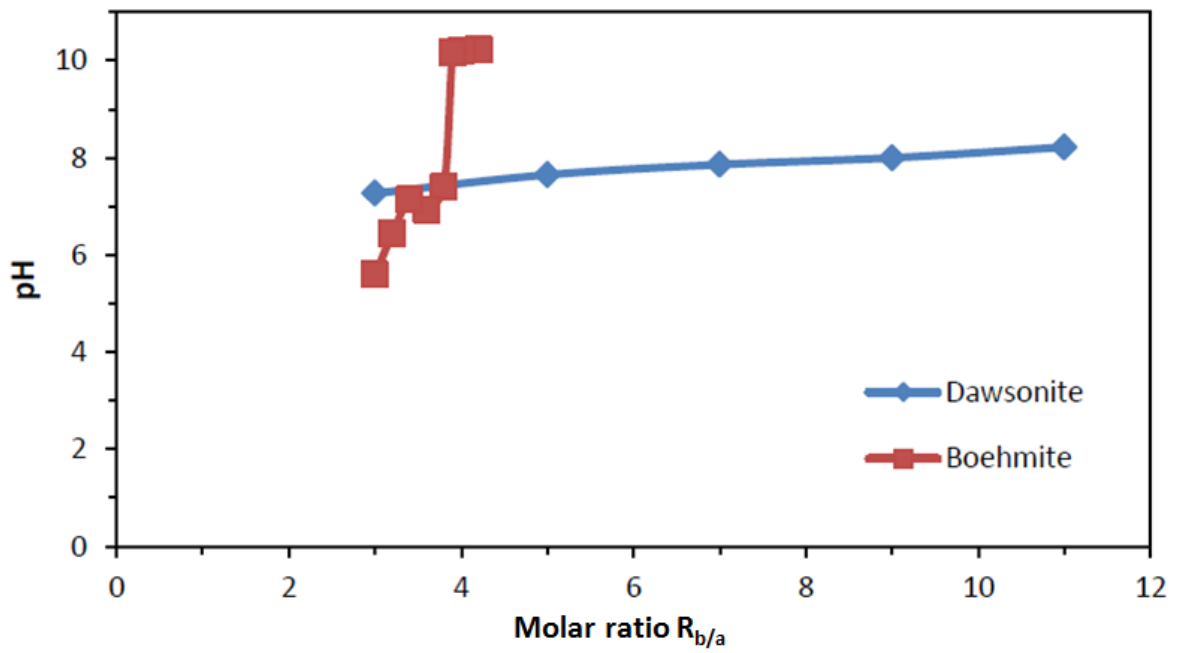


Figure S3. Evolution of the pH value as a function of molar ration  $R_{b/a}$  for boehmite and dawsonite synthesis